Hyperfine Interact
DOI 10.1007/s10751-011-0418-1

How Mössbauer spectroscopy can improve Li-ion batteries

Pierre-Emmanuel Lippens · Mohammed El Khalifi · Mohamad Chamas · Alexis Perea · Moulay-Tahar Sougrati · Costana Ionica-Bousquet · Laurent Aldon · Josette Olivier-Fourcade · Jean-Claude Jumas

Abstract In the domain of Li-ion batteries, Mössbauer spectroscopy is mainly used for the characterization of electrode materials and the analysis of electrochemical reactions. Depending on the properties under investigation, different approaches are often considered, which are based on *ex situ, in situ* and *operando* measurements. The specific electrochemical cells and sample preparations used for such measurements are described in this paper. Applications to selected examples of cathode and anode materials are presented in order to show how Mössbauer spectroscopy, when associated with other techniques, provides essential information to understand the mechanisms and improves the performances of Li-ion batteries.

Keywords Mössbauer spectroscopy · In situ · Operando · Li-ion batteries · Electrode materials · $LiFePO_4$ · Tin · Intermetallics

1 Introduction

New energy productions are crucial not only for the preservation of environment but also for the development of our societies since fossil fuel reserves will dry up in a near future. The recent development of renewable and intermittent energies based on sunlight or wind and the growth of new needs such as clean vehicles or portable electronics require new electrical energy storage systems. Thus, there is a strong demand for electrochemical systems and Li-ion batteries are, at the present time, one of the most interesting systems in terms of performances. Most of the research works are focused on new materials in order to increase energy density, reduce aging phenomena, lower the cost and improve safety [1].

P.-E. Lippens (✉) · M. El Khalifi · M. Chamas · A. Perea · M.-T. Sougrati · C. Ionica-Bousquet · L. Aldon · J. Olivier-Fourcade · J.-C. Jumas
Institut Charles Gerhardt, UMR CNRS 5253, Equipe Agrégats Interface et Matériaux pour l'Energie, Université Montpellier 2, CC1502, 34095 Montpellier Cedex 5, France
e-mail: lippens@univ-montp2.fr

Published online: 07 December 2011

The energy density of a Li-ion cell increases with both the electrode potential difference and the specific capacity of the electrodes. Compared to the present materials, it is in principle possible, but rather difficult, to increase the specific capacity of the cathode while it is not possible to decrease the potential of the anode. Thus, the best way to increase the energy density is to look for high potential cathodes and high capacity anodes. In order to find new electrode materials and improve their performances it is important to understand the electrochemical reactions that take place during the charge-discharge cycles. This is not an easy task because the electrochemical cells are rather complex systems composed by composite electrodes, multicomponent electrolyte, current collectors, etc. Thus, it is essential to combine different techniques and perform *in situ* and *operando* measurements for a reliable analysis of such mechanisms.

X-ray diffraction (XRD) is certainly the most commonly used technique to study electrode materials. Such a technique provides useful information on mechanisms involving crystalline phases but is of poor interest when the materials are amorphous and/or nanostructured, which is often the case with Li-ion batteries. Thus, atomic scale characterization is important in this respect, especially with element sensitive techniques, in order to follow local changes due to reactions of the electrode materials with lithium or aging processes [2]. Since many new electrode materials contain iron or tin atoms, Mössbauer spectroscopy can be used for such characterizations [3–7]. Combined with other experimental tools such as XRD, X-ray photoemission spectroscopy (XPS), X-ray absorption spectroscopy (XAS) or magnetic measurements it is then possible to give a consistent description of the phenomena which can be furthermore compared to theoretical models.

In this paper, we will show from some selected examples how Mössbauer spectroscopy can improve the performances of electrode materials for Li-ion batteries. Specific electrochemical cells are presented and applications of Mössbauer spectroscopy to new and promising cathode materials: lithium metal phosphates and anode materials: tin based intermetallics are discussed.

2 Experimental method

Mössbauer measurements can be made *ex situ* on electrode materials extracted from the electrochemical cell, *in situ* on material in the cell and *operando* on material in the cell during charge-discharge cycles. The two latter modes provide the most useful information that is directly related to changes within the cell. *Operando* mode allows to continuously study the electrochemical reactions with lithium. For example, in galvanostatic mode a constant current is applied to the cell and the Mössbauer spectra are recorded during cycling. *In situ* mode has a more general meaning since it also includes studies of the electrode material in the cell at a given stage of lithiation as a function of time, temperature, etc.

Different types of cells have been proposed for *in situ* experiments with batteries. To our knowledge, the first *in situ* Mössbauer experiments were performed by Geronov et al. for the investigation of an iron electrode in alkaline solution [8], three years before the first XRD *in situ* measurements [9]. Two decades after the Geronov's cell, Dunlap et al. proposed an *in situ* cell based on commercial 2325 cell in order to study Li-ion batteries [10, 11]. A cylindrical cell was used by Wattiaux

et al. [12] and an aluminium-laminated polyethylene bag by Ariyoshi et al. [13]. In our group, we have performed Mössbauer experiments with three kinds of cells. In the past, we used Bellcore plastic Li-ion batteries [14] for tin based anodes [15–17]. Such a cell can be easily used with a Mössbauer experimental set-up but requires specific technology and a rather high amount of electrochemically active material compared to other cells. We use now two other kinds of cell depending on the main electrochemical mechanisms that take place in the electrode materials.

The first cell was initially developed for *in situ* XRD and XAS measurements in transmission or reflection geometry and a detailed description is given in Ref. [18]. The modified XRD-XAS cell can be easily used with powdered electrode materials if only a rather small pressure is required to maintain electrical contacts between particles. This is the case of insertion materials in which electrochemical mechanisms are governed by topotactic reactions and to a great extent when electrochemical reactions take place with small volume variations.

The second cell was adapted from a Swagelok-type cell which is commonly used for electrochemical tests of Li-ion batteries. Such a cell presents easily achieved proper installation, excellent gas-tight sealing and low cost. It can be easily used with powdered electrode materials even when electrochemical reactions take place with volume variations such as alloying or conversion reactions. The cell is made of the commercially available Swagelok tube union made of perfluoroalkoxy polymer and stainless steel tubes with extremities formed by PMMA γ-transparent windows. The anode is made of a thin lithium foil of high quality in contact with the stainless steel tube and the cathode is formed by powdered active material pressed against a beryllium foil used as a connector.

For *in situ* and *operando* measurements, the cells are placed between the γ-rays source and the detector. The measurements are usually performed under galvanostatic conditions with a Biologic SP-150 potentiostat. The Mössbauer data are recorded during several hours (depending on the Li rate and the required signal-to-noise ratio), saved and then the memory is cleaned and so on. Each spectrum is collected during the reaction of a small number of lithium, typically lower than 0.1 Li per active center (0.05 Li for $LiFePO_4$ and 0.1Li for $FeSn_2$). This means that Mössbauer data are collected continuously during the charge-discharge cycles, which justifies the use of "operando" term for such experiments. A conventional Mössbauer experimental set-up is used for such measurements [16].

3 Application to cathode materials

Commonly used cathode materials are lithium-metal oxides but there is an increasing interest for lithium metal phosphates with olivine structure like $LiFePO_4$ [19–22]. $LiFePO_4$ is inexpensive, environmentally friendly, safe, with good cycle life and high specific capacity compared to other cathode materials. In addition, the potential ($\sim$3.4 V v.s. Li^+/Li^0) can be increased by substituting another transition metal for Fe. However, $LiFePO_4$ is a wide band gap semiconductor and must be used as powdered nanoparticles with carbon coating for a good electrical percolation [23] although cation doping can also increase the electronic conductivity [24]. The performances also depend on intrinsic defects like Li/Fe antisites but also on impurities like iron oxides or iron phosphides that can be formed during the synthesis depending on the

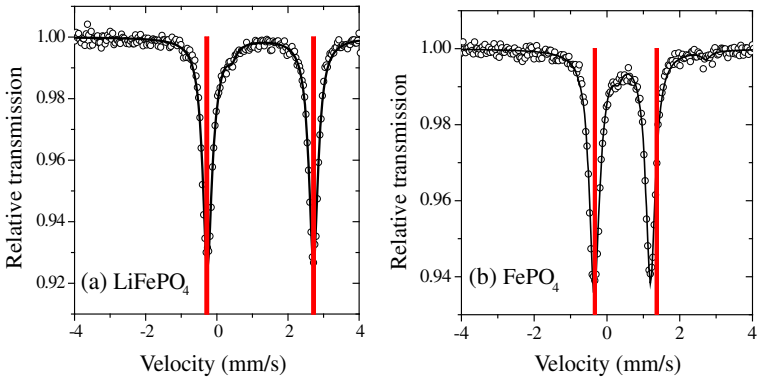

Fig. 1 ^{57}Fe Mössbauer spectra of $LiFePO_4$ (**a**) and $FePO_4$ (**b**); Comparison between experimental data at room temperature (*black circles*) and DFT calculations (*red vertical lines*)

experimental conditions. The characterization of the pristine material, the analysis of the charge-discharge mechanisms and the influence of defects can be studied by ^{57}Fe Mössbauer spectroscopy and we present here several applications of this technique.

At room temperature, the ^{57}Fe Mössbauer spectra of both $LiFePO_4$ and $FePO_4$ are formed by doublets. For $LiFePO_4$, the experimental values of the isomer shift and quadrupole splitting are $\delta = 1.22$ mm/s and $\Delta = 2.96$ mm/s, respectively. These values are close to those obtained by DFT calculations, taking into account both the spin polarization and the correlation of the Fe 3d electrons (Fig. 1a). This can be interpreted from the Fe^{2+} high spin configuration of the iron atoms in distorted octahedral environments formed by oxygen atoms. The charge (delithiation) leads to olivine $FePO_4$ with Mössbauer parameters $\delta = 0.45$ mm/s and $\Delta = 1.53$ mm/s close to the DFT values (Fig. 1b). Compared to $LiFePO_4$, the value of δ decreases because the extraction of one lithium is accompanied with the decrease of one Fe3d$\downarrow$ electron per Fe, changing high spin Fe^{2+} (in $LiFePO_4$) into high spin Fe^{3+} (in $FePO_4$). This affects the electronic structure near the Fermi level as shown by XPS and DFT calculations [25]. The observed decrease of Δ is also related to the decrease of one Fe 3d electron per Fe that strongly influences the Fe 3d electron density shape.

The reversible charge-discharge cycles have been studied by *operando* ^{57}Fe Mössbauer spectroscopy by different authors and interpreted as $LiFePO_4/FePO_4$ two-phase reactions [26, 27]. The substitution of Fe by Mn ($LiFe_{1-x}Mn_xPO_4$) increases the voltage from 3.4 V vs. Li^+/Li^0 to 4.1 V vs. Li^+/Li^0. Unfortunately, the full substitution ($x = 1$) leads to capacity fading that could be due to structural instability (the Jahn-Teller distortion around Mn^{3+} ions in $MnPO_4$) and low conductivity [28]. Better rate capabilities have been obtained with partial Fe/Mn substitution but the potential profile is formed by two plateaus at about 3.5 V and 4 V vs. Li^+/Li^0 due to the Fe^{3+}/Fe^{2+} and Mn^{3+}/Mn^{2+} redox reactions, respectively. A two dimensional phase diagram of $Li_yFe_xMn_{1-x}PO_4$ as a function of (x,y) ($0 \leq x,y \leq 1$) has been proposed by Yamada et al. [29]. We have obtained similar results and we briefly summarize here, as an example, the mechanism obtained for $Li_yFe_{0.75}Mn_{0.25}PO_4$ by *operando* ^{57}Fe Mössbauer spectroscopy with the XRD-XAS modified cell described above. The electrochemical curve shows the expected two plateaus although the potentials are different for the charge and the discharge because of polarization

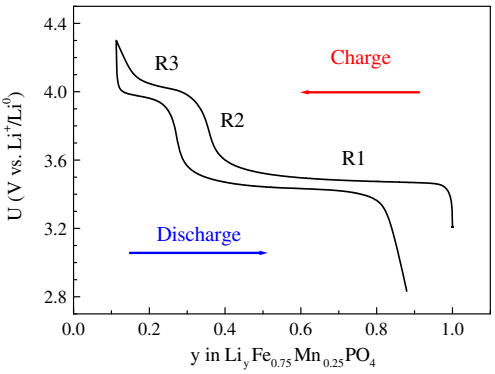

Fig. 2 Potential curve of the first charge-discharge cycle for $LiFe_{0.75}Mn_{0.25}PO_4$ in modified XRD-XAS cell at C/40. R1-R3 denote the three regions discussed in the text

effects (Fig. 2). Three regions can be defined by considering the transition between the two plateaus.

The three regions were unambiguously distinguished from *operando* XRD which clearly shows, for the charge, two-phase regions for $y \leq 0.25$ (Region R3) and $0.55 \leq y \leq 1$ (Region R1), and a single-phase region for $0.25 \leq y \leq 0.55$ (Region R2). The ^{57}Fe Mössbauer spectra obtained at room temperature for the first cycle are shown in Fig. 3.

The first spectrum ($y = 0$) is formed by a doublet ($\delta = 1.23$ mm/s and $\Delta = 2.95$ mm/s), similar to that of $LiFePO_4$, that can be assigned to high spin Fe^{2+}. At the end of the region R1 ($y = 0.55$), the spectrum can be fitted with two doublets that can be attributed to Fe^{2+} ($\delta = 1.28$ mm/s and $\Delta = 2.71$ mm/s) and Fe^{3+} ($\delta = 0.43$ mm/s and $\Delta = 1.1$ mm/s). Thus, a mixed valence phase was formed during the delithiation of $LiFe_{0.75}Mn_{0.25}PO_4$. All the intermediate spectra in R1 were fitted with these contributions and reaction in R1 can be written

$$\begin{aligned} LiFe^{2+}_{0.75}Mn^{2+}_{0.25}PO_4 \leftrightarrow\ & (1-y)\,Li + 2.22\,(y-0.55)\,LiFe^{2+}_{0.75}Mn^{2+}_{0.25}PO_4 \\ & +2.22\,(1-y)\,Li_{0.55}Fe^{2+}_{0.3}Fe^{3+}_{0.45}Mn^{2+}_{0.25}PO_4 \\ & \text{with } 0.55 \leq y \leq 1 \end{aligned} \tag{1}$$

The second region R2 ($0.25 \leq y \leq 0.55$) is characterized by a strong increase of the potential up to about 4.0 V. A systematic shift of the (200) diffraction peak at $2\theta \sim 29.5°$ of the phase $Li_{0.55}Fe^{2+}_{0.3}Fe^{3+}_{0.45}Mn^{2+}_{0.25}PO_4$ suggests a solid solution in this region. The relative contribution of Fe^{2+} to the Mössbauer spectra decreases whereas that of Fe^{3+} increases. The Mössbauer parameters do not change significantly except for the quadrupole splitting of Fe^{3+} that increases gradually (22%) with the oxidation of iron. This indicates significant lattice changes in agreement with XRD results. Thus, the extraction of lithium in region R2 changes the oxidation state from Fe^{2+} to Fe^{3+}, which also causes modifications of the Fe 3d electron density shape around Fe^{3+}, following the single-phase reaction:

$$\begin{aligned} Li_{0.55}Fe^{2+}_{0.3}Fe^{3+}_{0.45}Mn^{2+}_{0.25}PO_4 \leftrightarrow\ & (0.55-y)\,Li + Li_yFe^{2+}_{y-0.25}Fe^{3+}_{1-y}Mn^{2+}_{0.25}PO_4 \\ & \text{with } 0.25 \leq y \leq 0.55 \end{aligned} \tag{2}$$

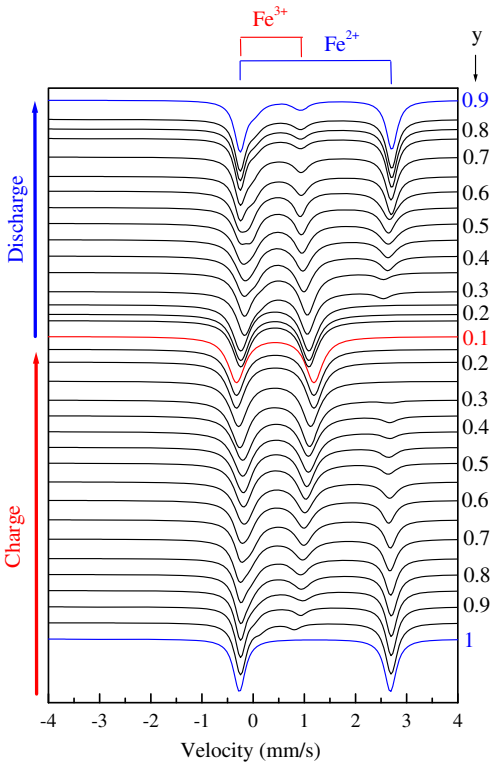

Fig. 3 ^{57}Fe Mössbauer spectra of $Li_yFe_{0.75}Mn_{0.25}PO_4$ (with $0.1 < y < 1$) in a modified XRD-XAS cell for *operando* measurements during the first cycle at C/40 and room temperature

Finally, the third region R3 ($0.1 \leq y \leq 0.25$) corresponds to the oxidation of Mn^{2+} into Mn^{3+} which occurs on the short potential plateau around 4.0 V. In this region, the first Mössbauer spectrum ($y = 0.25$) with Mössbauer parameters: $\delta = 0.41$ mm/s and $\Delta = 1.30$ mm/s can be assigned to $Li_{0.25}Fe^{3+}_{0.75}Mn^{2+}_{0.25}PO_4$ and the last one reflects the contribution of both this compound and the fully delithiated compound $Fe^{3+}_{0.75}Mn^{3+}_{0.25}PO_4$ ($\delta = 0.41$ mm/s and $\Delta = 1.52$ mm/s). The two-phase reaction in this region can be written

$$Li_{0.25}Fe^{3+}_{0.75}Mn^{2+}_{0.25}PO_4 \leftrightarrow (0.25 - y)\, Li + 4y\, Li_{0.25}Fe^{3+}_{0.75}Mn^{2+}_{0.25}PO_4 + 4(0.25 - y) \times Fe^{3+}_{0.75}Mn^{3+}_{0.25}PO_4 \text{ with } 0 \leq y \leq 0.25 \quad (3)$$

The overall mechanism is reversible and is also observed for the discharge. It strongly differs from the two-phase reaction in $LiFePO_4$.

Mössbauer spectroscopy is also widely used to characterize the pristine materials in order to optimize the electrochemical performances. As an example, an asymmetric broadening of the low velocity peak of the Mössbauer spectrum of $LiFePO_4$ is often observed, as shown for samples obtained in tube furnace under argon flow (Fig. 4). Such spectrum can be fitted with the main sub-spectrum due to $LiFePO_4$ (88%) and a two-component sub-spectrum that can be assigned to Fe_2P (12%). The latter compound must be considered as an impurity that decreases the specific capacity of the electrode. It is due to reducing synthesis conditions (Ar/H_2 flux) and forms a surface layer that must be as thin as possible [30].

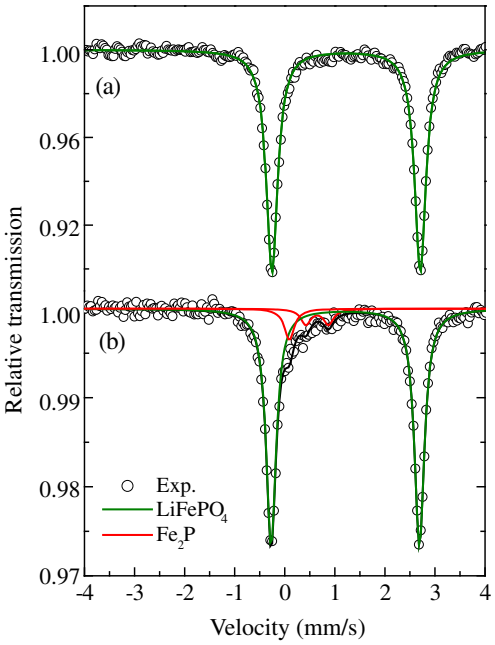

Fig. 4 ^{57}Fe Mössbauer spectra of two samples of $LiFePO_4$ obtained with different synthesis conditions: pure $LiFePO_4$ (**a**) and $LiFePO_4$ with Fe_2P impurity (**b**)

4 Application to anode materials

The most commercially used anodes for Li-ion batteries are made from carbon or titanates. The electrochemical reaction mechanisms are based on reversible insertion of Li ions in the host material and the energy density is limited by the small number of inserted Li. For example, only 1 Li per 6 C can be intercalated into graphite, which gives a specific capacity of 370 Ah/kg. In order to overcome this limitation, materials that reversibly react with lithium by alloying-dealloying processes or by conversion reactions have been proposed. Si and βSn are promising high capacity anode materials that form alloys with lithium and their theoretical specific capacities are 4200 Ah/kg and 990 Ah/kg, respectively. However, alloying reactions suffer for large volume variations leading to poor cycling performances. To minimize the structural instabilities, different strategies have been considered for βSn, such as nanosized tin [31], tin oxides [32], tin composite oxides (TCO) [33], metallic tin dispersed in a composite oxide [34–36] and tin-metal alloys. In the latter case, tin is associated with an electrochemically inactive metal that is expected to be extruded during the first discharge from the pristine materials in order to form metallic nanoparticles that buffer volume variations. Different metals have been considered including Cu [37], Ni [38–40], Co [41, 42], Fe [43–45] or Nb [46]. The case of Co is of particular interest and Sony commercialized in 2005 the Nexelion battery with a Co-Sn-C amorphous anode improving the capacity of the battery by 30% compared to other systems [47–51]. However, the replacement of Co by another metal such Fe might reduce the cost of the electrode materials and improve the environmental impact [52]. We present here some results for $FeSn_2$ which is the tin richest binary compound with Fe and has a maximum theoretical capacity of about 800 Ah/kg (for 4.4 Li/Sn).

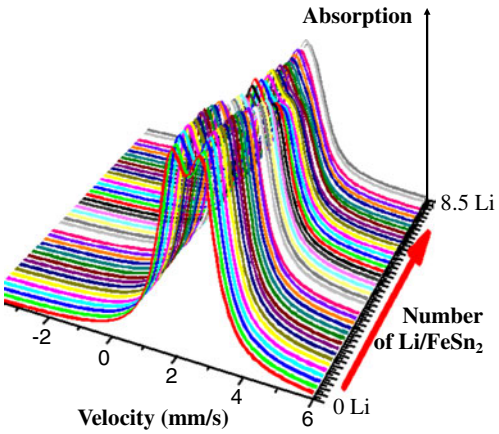

Fig. 5 ^{119}Sn Mössbauer spectra of nanostructured $FeSn_2$ in modified Swagelok cell for *operando* measurements during the first discharge at C/10 and room temperature

This compound is of particular interest since it can be easily nanostructured, which increases the specific surface area of the active material. It can be considered as a reference compound for transition metal-tin intermetallics as anode materials since the reaction mechanisms are very similar. And last but not least, it contains two Mössbauer isotopes ^{57}Fe and ^{119}Sn.

The electrochemical tests and the study of the mechanisms were performed with a composite electrode formed by nanostructured $FeSn_2$ (80 wt.%), polytetrafluoroethylene as binder (10 wt.%) and carbon black (SP) as conductive additive (10 wt.%). About 8 Li/$FeSn_2$ reacted with the electrode during the first discharge at a rate of C/10 [45]. ^{119}Sn Mössbauer *operando* measurements were performed with the modified Swagelok-type cell at room temperature (Fig. 5). The spectrum of the pristine material is formed by a doublet ($\delta = 2.2$ mm/s, $\Delta = 0.9$ mm/s) which is transformed into a single and slightly asymmetric peak at the end of the discharge [45]. The latter peak was fitted with two components ($\delta = 1.88$ mm/s, $\Delta = 0.2$ mm/s and $\delta = 1.96$ mm/s, $\Delta = 0.7$ mm/s) that can be attributed to Li_7Sn_2 nanoparticles [53, 54]. The composition of this Li-Sn alloy differs from the expected maximum composition ($Li_{22}Sn_5$) reducing the specific capacity of the electrode by about 20%. All the other spectra obtained during the discharge were successfully fitted by considering these two contributions.

The relative amounts of $FeSn_2$ and Li_7Sn_2 were evaluated from the relative subspectrum areas and the ratio of the Lamb-Mössbauer factors of these two materials (Fig. 6).

The observed linear variations indicate that the first discharge can be described by the conversion reaction

$$FeSn_2 + 7Li \rightarrow Fe + Li_7Sn_2 \tag{4}$$

Thus, nanostructured $FeSn_2$ is directly transformed into Li_7Sn_2 nanoparticles without the intermediate Li-Sn phases observed for βSn anode material [55].

The iron particles formed during the discharge were characterized from magnetic measurements for the fully lithiated electrode material. The variations of the magnetization as a function of the magnetic field, H, at different temperatures show change from ferromagnetic to superparamagnetic regime at about 20 K. The saturation

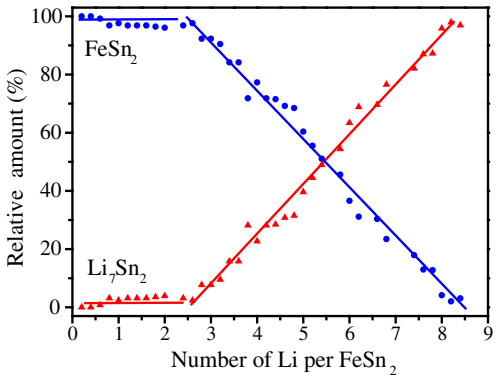

Fig. 6 Relative amounts of $FeSn_2$ (*blue circles*) and Li_7Sn_2 (*red triangles*) evaluated from *operando* ^{119}Sn Mössbauer measurements during the first discharge as a function of the number of Li per $FeSn_2$

magnetization at H = 5T and T = 5K is of about 220 Am^2/kg and is close to that of bulk α-Fe. This suggests that nanoparticles are coated with a non-magetic layer as expected for the surface electrolyte interphase (SEI) previously observed by XPS [39, 45]. In the superparamagnetic regime, the magnetization curves were fitted with a Langevin function in order to evaluate the iron nanoparticle diameter. The obtained value of about 3 nm is consistent with ZFC-FC measurements. Thus, the averaged iron nanoparticle size is constant during the first discharge.

The ^{119}Sn Mössbauer spectra are strongly modified if nanostructured $FeSn_2$ is replaced by $FeSn_2$ microparticles as active material in the pristine electrode. This is due to the size/cristallinity of the particles that allows observing transferred hyperfine field. The Mössbauer spectrum obtained at the end of the discharge is similar to that observed for nanostructured $FeSn_2$ and can also be assigned to Li_7Sn_2. The other spectra of the discharge can be fitted with these two contributions (Fig. 7).

Thus, the same basic reaction mechanism is obtained for the two types of $FeSn_2$ pristine materials: the first discharge transforms $FeSn_2$ into a nanocomposite Fe/Li_7Sn_2. This nanocomposite should be considered as the real starting electrode material. The behaviour of the battery on cycling depends on the first discharge which is a crucial restructuring step. For example, high rate cycling requires a first low rate discharge [56].

By combining ^{57}Fe and ^{119}Sn Mössbauer experiments, we have found that the following cycles consist in dealloying of Li_7Sn_2 leading to Li-rich Li_xSn alloys (on charge) followed by alloying of Li-rich Li_xSn alloys up to Li_7Sn_2 (on discharge). The iron nanoparticles did not react with Sn at the electrochemical regimes considered in our experiments (C/10–10C) and acted as a buffer to limit the volume variations as expected. However, a capacity fading generally occurs after 50 cycles because of the loss of electrical contacts during the charge-discharge cycles and the growth/coalescence of the particles, as shown by *in situ* Mössbauer experiments [45]. The capacity fading is observed for all the tin based intermetallics although it can be reduced by optimizing the electrode formulation or the material composition [48, 57, 58]. Although the reaction mechanisms are similar for the other transition metals, back reactions of tin with the metallic nanoparticles were often observed by Mössbauer spectroscopy during the charge. For example, Ni_3Sn_4 is reformed at the end of charge [39], while a complex Co-Sn-Li alloy is obtained with $CoSn_2$ pristine material [16]. Even in the case of $FeSn_2$, back reaction of Fe with Sn has been

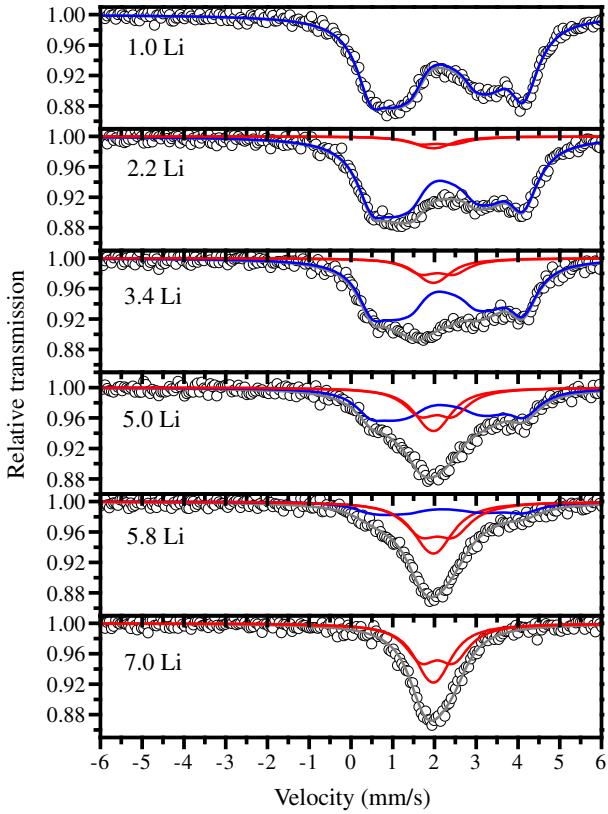

Fig. 7 Selected ^{119}Sn Mössbauer spectra of microsized $FeSn_2$ based electrode in modified Swagelok cell for *operando* measurements during the first discharge at C/10 and room temperature. The spectra were fitted with the contributions of $FeSn_2$ (*blue*) and Li_7Sn_2 (*red*)

observed, but at very low lithium rate [59]. Thus, both the nature of the metal and the electrochemical test conditions affect the charge process. However, it is still not clear whether cycling performances are improved with inactive metallic nanoparticles that buffer the volume variations of Li-Sn alloys or with metallic nanoparticles trapping Sn during the charge to avoid the formation of βSn or poorly lithiated Li-Sn alloys.

5 Conclusion

Mössbauer spectroscopy provides useful and detailed information on electrode materials for Li-ion batteries and electrochemical reaction mechanisms that is essential to improve the performances as energy density, cycling capability or safety. *In situ* and *operando* measurements are crucial for such characterizations since they allow continuous measurements during current flow and avoid extraction of the materials from the electrochemical cell. It is possible to follow redox reactions, changes in local electronic structure and local environments of the Mössbauer isotopes, formation of amorphous and nanocristalline phases during charge-discharge cycles, but also to detect impurities in the pristine materials or to analyse phase instability as a function of time due to aging phenomena.

However, Mössbauer spectroscopy must be combined with other techniques, including theoretical approaches, for the analysis of the complex mechanisms that take place within or at the surface of the electrode particles. At this condition, it will be possible to improve performances and find new electrode materials for the future energy storage systems.

Acknowledgement This work has been carried out in the framework of the European Research Institute ALISTORE. The authors would like to thank SAFT Company Bordeaux (contract 02988) for the financial support.

References

1. Tarascon, J.M.: Phil. Trans. Royal Soc. A **368**, 3227 (2010)
2. Naille, S., Dedryvère, R., Zitoun, D., Lippens, P.E.: J. Power Sources **189**, 814 (2009)
3. Lippens, P.E., Jumas, J.C. (Guest Ed.): It's all about the battery. Mössbauer Eff. Ref. Data J., **33**(2) (2010)
4. Jumas, J.-C., Womes, M., Lippens, P.E., Olivier-Fourcade, J.: Hyperfine Interact. **182**, 103 (2008)
5. Robert, F., Lippens, P.E., Olivier-Fourcade, J., Jumas, J.C., Morcrette, M.: J. Power Sources **146**, 492 (2005)
6. Aldon, L., Kubiak, P., Picard, A., Lippens, P.E., Jumas, J.C., Olivier-Fourcade, J.: Hyperfine Interact. **156**, 497 (2004)
7. Lippens, P.E., Jumas, J.C.: Nanocomposites, Ionic Conducting Materials and Structural Spectroscopies. Springer, Series: Electronic Materials: Science & Technology, Vol. 10, Knauth, Philippe; Schoonman, Joop (Eds.), ISBN: 978-0-387-33202-4, p. 247–272 (2008)
8. Geronov, Y., Tomov, T., Georgiev, S.: J. Appl. Electrochem. **5**, 351 (1975)
9. Chianelli, R.R., Scanlon, J.C., Rao, B.M.L.: J. Electrochem. Soc. **125**, 1563 (1978)
10. Mao, O., Dunlap, R.A., Courtney, I.A., Dahn, J.R.: J. Electrochem. Soc. **145**, 4195 (1998)
11. Dunlap, R.A., Obrovac, M.N., Li, J., Smith, A., Hatchard, T.D., Sanderson, R.J., Dahn, J.R.: Mössbauer Eff. Ref. Data J. **33**, 32 (2010)
12. Wattiaux, A., Fournès, L., Delmas, C.: Mössbauer Eff. Ref. Data J. **33**, 37 (2010)
13. Ariyoshi, K., Ohzuku, T.: Mössbauer Eff. Ref. Data J. **33**, 43 (2010)
14. Tarascon, J.M., Gozdz, A., Schmutz, C., Shokoohi, F., Warren, P.C.: Solid State Ionics **86**, 49 (1996)
15. Aldon, L., Ionica, C., Lippens, P.E., Morcrette, M., Larcher, D., Tarascon, J.M., Jumas, J.C.: Hyperfine Interact. **167**, 729 (2006)
16. Bousquet, C.M., Lippens, P.E., Aldon, L., Olivier-Fourcade, J., Jumas, J.C.: Chem. Mater. **18**, 6442 (2006)
17. Aboulaich, A., Robert, F., Lippens, P.E., Aldon, L., Olivier-Fourcade, J., Willmann, P., Jumas, J.C.: Hyperfine Interact. **167**, 733 (2006)
18. Leriche, J.B., Hamelet, S., Shu, J., Morcrette, M., Masquelier, C., Ouvrard, G., Zerrouki, M., Soudan, P., Belin, S., Elkaïm, E., Baudelet, F.: J. Electrochem. Soc. **157**, A606 (2010)
19. Pahdi, A.K., Nanjundaswami, K.S., Goodenough, J.B.: J. Electrochem. Soc. **144**, 1188 (1997)
20. Yamada, A., Chung, S.C., Hinokuma, K.: J. Electrochem Soc. **48**, A224 (2001)
21. Shiratsuchi, T., Okada, S., Yamaki, J.I., Yamashita, S., Nishida, T.: J. Power Sources **173**, 979 (2007)
22. Zhang, W.J.: J. Power Sources **196**, 2962 (2011)
23. Julien, C.M., Mauger, A., Zaghib, K.: J. Mater. Chem. **21**, 9955 (2011)
24. Wagemaker, M., Ellis, B.L., Luetzenkirchen-Hecht, D., Mulder, F.M., Nazar, L.F.: Chem. Mater. **20**, 6313 (2008)
25. Castro, L., Dedryvère, R., El Khalifi, M., Lippens, P.E., Bréger, J., Tessier, C., Gonbeau, D.: J. Phys. Chem C **114**, 17995 (2010)
26. Andersson, A.S., Kalska, B., Häggström, L., Thomas, J.O.: Solid State Ionics **130**, 41 (2000)
27. Aldon, L., Perea, A., Womes, M., Ionica-Bousquet, C.M., Jumas, J.-C.: J. Solid State Chem. **183**, 218 (2010)
28. Yamada, A., Hosoya, M., Chung, S.C., Kudo, Y., Hinokuma, K., Liu, K.Y., Nishi, Y.: J. Power Sources **119**, 232 (2003)
29. Yamada, A., Kudo, Y., Liu, K.Y.: J. Electrochem. Soc. **148**, A1153 (2001)

30. Rho, Y.H., Nazar, L., Perry, L., Ryan, D.: J. Electrochem. Soc. **154**, A283 (2007)
31. Wang, F., Zhao, M.S., Song, X.P.: J. Power Sources **175**, 558 (2008)
32. Chouvin, J., Olivier-Fourcade, J., Jumas, J.C., Simon, B., Biensan, P.H., Madrigal, F.J.F., Tirado, J.L., Vicente, C.P.: J. Electroanal. Chem. **494**, 136 (2000)
33. Idota, Y., Kubota, T., Matsufuji, A., Maekawa, Y., Miyasaka, T.: Science **276**, 1395 (1997)
34. Zheng, Y., Yang, J., Nuli, Y.N., Wang, J.L.: J. Power Sources **174**, 624 (2007)
35. Aboulaich, A., Mouyane, M., Robert, F., Lippens, P.E., Olivier-Fourcade, J., Willmann, P., Jumas, J.C.: J. Power Sources **174**, 1224 (2007)
36. Mouyane, M., Lippens, P.E., Womes, M., Ducourant, B., Willmann, P., Olivier-Fourcade, J.: Hyperfine Interact. **187**, 27 (2008)
37. Naille, S., Dedryvère, R., Leroy, S., Martinez, H., Lippens, P.E., Jumas, J.C., Gonbeau, D.: J. Power Sources **174**, 1086 (2007)
38. Naille, S., Lippens, P.E., Morato, F., Olivier-Fourcade, J.: Hyperfine Interact. **167**, 785 (2006)
39. Ehinon, K.K.D., Naille, S., Dedryvère, R., Lippens, P.E., Jumas, J.C., Gonbeau, D.: Chem. Mater. **20**, 5388 (2008)
40. Hassoun, J., Panero, S., Simon, P., Taberna, P.L., Scrosati, B.: Advanced Mat. **19**, 1632 (2007)
41. Alcantara, R., Rodriguez, I., Tirado, J.L.: Chem. Phys. Chem. **9**, 1171 (2008)
42. He, J., Zhao, H., Wang, J., Chen, J.: J. Alloys Compd. **508**, 629 (2010)
43. Mao, O., Dunlap, R.A., Dahn, J.R.: Solid State Ionics **118**, 99 (1999)
44. Nwokeke, U.G., Alcántara, R., Tirado, J.L., Stoyanova, R., Zhecheva, E.: J. Power Sources **196**, 6768 (2011)
45. Chamas, M., Lippens, P.E., Jumas, J.C., Boukerma, K., Dedryvère, R., Gonbeau, D., Hassoun, J., Panero, S., Scrosati, B.: J. Power Sources **196**, 7011 (2011)
46. Naille, S., Mouyane, M., El Amraoui, M., Lippens, P.-E., Jumas, J.-C., Olivier-Fourcade, J.: Hyperfine Interact. **187**, 19 (2008)
47. Sony, U.S. Patent 0053131
48. Ferguson, P.P., Martine, M.L., George, A.E., Dahn, J.R.: J. Power Sources **194**, 794 (2009)
49. Ferguson, P.P., Todd, A.D.W., Dahn, J.R.: Electrochem. Commun. **10**, 25 (2008)
50. Ortiz, G.F., Alcántara, R., Rodríguez, I., Tirado, J.L.: J. Electroanal. Chem. **605**, 98 (2007)
51. Hassoun, J., Panero, S., Mulas, G., Scrosati, B.: J. Power Sources **171**, 928 (2007)
52. Nwokeke, U.G., Chadwick, A.V., Alcántara, R., Alfredsson, M., Tirado, J.L.: J. Alloys Compd. **509**, 3074 (2011)
53. Robert, F., Lippens, P.E., Fourcade, R., Jumas, J.C., Morcrette, M., Tarascon, J.M.: Hyperfine Interact. **167**, 797 (2006)
54. Robert, F., Lippens, P.E., Olivier-Fourcade, J., Jumas, J-C., Gillot, F., Morcrette, M., Tarascon, J-M.: J. Solid State Chem. **180**, 339 (2007)
55. Lippens, P.E., Aldon, L., Ionica, C.M., Robert, F., Olivier-Fourcade, J., Jumas, J.C.: Characterization of Li insertion mechanisms in negative electrode materials for Li-ion batteries by Mössbauer spectroscopy and first-principles calculations. In: Knauth, P., Masquelier, C., Traversa, E., Wachsman, E.D. (eds.) Solid State Ionics 2004. Materials Research Society Symposium Proceedings, vol. 835, pp. 249–260. Materials Research Society, Warrendale (2005)
56. Chamas, M., Lippens, P-E., Jumas, J-C., Hassoun, J., Panero, S., Scrosati, B.: Electrochim. Acta **56**, 6732 (2011)
57. Sivasankaran, V., Marino, C., Chamas, M., Soudan, P., Guyomard, D., Jumas, J.C., Lippens, P.E., Monconduit, L., Lestriez, B.: J. Mater. Chem **21**, 5076 (2011)
58. Li, J., Le, D.B., Ferguson, P.P., Dahn, J.R.: Electrochim. Acta 55, 2991 (2010)
59. Dunlap, R.A., Mao, O., Dahn, J.R.: Phys. Rev. B **59**, 3494 (1999)